Controlled removal of toxic harmful algal bloom species, *Alexandrium minutum* using rice husk ash silica/chitosan film reinforced with (3-glycidyloxypropyl)triethoxysilane and glycerol

Anwar Iqbal[1*], Nur Hanisah Ibrahim[1], Normawaty Mohammad-Noor [2] , Roziawati Mohd Razali [3], Dede Heri Yuli Yanto [4,5], Lee D. Wilson[6], He Ranri[1]

[1] School of Chemical Sciences, Universiti Sains Malaysia, Minden, Gelugor 11800, Penang, Malaysia

[2] Department of Marine Science, Kulliyyah of Science, International Islamic University Malaysia, Jalan Sultan Ahmad Shah, Bandar Indera Mahkota, Kuantan 25200, Pahang, Malaysia

[3] Fisheries Research Institute (FRI), Department of Fisheries Malaysia, Batu Maung 11960, Penang

[4] Research Center for Applied Microbiology, National Research and Innovation Agency (BRIN), Cibinong, Bogor 16911, Indonesia

[5] Research Collaboration Center for Marine Biomaterials, Jatinangor 45360, Indonesia

[6] Department of Chemistry, University of Saskatchewan, 110 Science Place, Room 165 Thorvaldson Building, Saskatoon, SK S7N 5C9, Canada

* Corresponding author's email: anwariqbal@usm.my

Abstract

Harmful algal blooms (HABs) pose significant threats to public health, tourism, fisheries, and ecosystems. This study investigates the use of rice husk ash silica/chitosan composite films reinforced with (3-glycidyloxypropyl)triethoxysilane (CHT/SiO_2/GPTEOS) and glycerol

(CHT/SiO_2/Gly) for the controlled removal of toxic HABs cells, *Alexandrium minutum*. IR spectral results confirm that crosslinking within the films occurs through condensation reactions and hydrogen bonding between silanol (Si-OH), hydroxyl (-OH), and amine (-NH_2) groups. The algal removal efficiency (RE;%) of CHT/SiO_2/Gly was 26.5±10.81%, while CHT/SiO_2/GPTEOS achieved a markedly higher RE of 50.06 ± 11.90%. The lower RE of CHT/SiO_2/Gly was attributed to the film's swelling, which allowed trapped algae cells to escape, and reduced electrostatic interactions between the negatively charged algae cells and the film surface. Digital microscopy analysis revealed that the algae cells attached to the CHT/SiO_2/Gly ruptured due to the stress exerted by the amine groups. Meanwhile, the structure of the algae cells remained intact on CHT/SiO_2/GPTEOS. The films were easily separated from the algae culture and exhibited excellent biodegradability, degrading completely within 30 days of burial in soil. These findings demonstrate the potential of CHT/SiO_2/GPTEOS as an environmentally sustainable material for recovery and mitigating effects of HABs.

Keywords: *Alexandrium minutum*; chitosan; glycerol; harmful algal bloom; silica; (3-glycidyloxypropyl)triethoxysilane

*Corresponding Author's email: anwariqbal@usm.my

1. Introduction

Proliferations of toxic and nontoxic microalgal groups (e.g. diatoms, dinoflagellates, raphidophytes, haptophytes, pelagophytes, cryptophytes) and a few macroalgal species of green or brown algae can give rise to an aquatic phenomenon known as harmful algal blooms (HABs) [1–4]. A single occasion of HABs can seriously affect public health, tourism, fisheries and ecosystems [5–7]. Humans and animals are exposed to the biotoxins of the toxin-producing algae by consuming contaminated seafood and water activities such as swimming and inhaling droplets containing the aerosolized biotoxin [8]. The non-toxic algae species can cause water discolouration and harm marine species through de-oxygenation of seawater, production of allelochemicals and mucus, or physical damage by spines or barbed setae [9–11]. The frequency of the HABs occurrence is attributed to an increase in eutrophication, climate change, transport and exchange of ballast water, and the development of the mariculture industry [12,13]. However, Hallegraeff et al. [14] presented a different opinion based on their study. They noted that the rise is likely due to improved monitoring rather than other factors. However, given the risks posed by HABs, it is critical to implement mitigation measures to reduce their occurrence and effects.

The use of natural clays as HABs mitigating agent was first introduced in the 1970's in the coastal water of Kagoshima, Japan [15]. However, the flocculation ability of the natural clays was very low and required a large quantity. Various organic and inorganic modifiers have been used to enhance the electrostatic attraction between the mitigating agent and the algae cells [16]. The suitability of materials for use as HABs mitigating agents depends on the materials' structure, particle size, effective interaction radius and surface charge [17]. The mitigation agents must have a higher positive charge to attract and capture the negatively

charged algae cells. The occurrence of repulsive forces between the materials and algae cells will reduce the flocculation efficiencies [18].

Polyaluminium chloride (PAC) is an effective flocculant to flocculate and remove suspended particles from water bodies. Reports have shown that modifying clays with PAC increased the surface charge from negative to positive and enhanced the clays' flocculation efficiency [19]. Chi et al. [20] reported that kaolin modified with PAC (PAC-MC) could effectively control *Karenia brevis* blooms and adsorb brevetoxins (BTXs) to less toxic derivatives due to the enhanced surface potential and binding sites. The adsorption was endothermic and conformed to pseudo-second-order adsorption kinetics ($k^2 = 6.8 \times 10^{-4}$, PAC-MC = 0.20 g L^{-1}) and the Freundlich isotherm (K_f = 55.30, 20 °C). Zhang et al. [21] tested two types of clays modified with PAC through the immersion method for the removal of *Aphanizomenon flos-aquae* blooms. The removal efficiency reached more than 90%. The effectiveness of the clay in controlling the bloom depends on its mineral composition, particle size, mineral-to-PAC ratio, and hydraulic shear.

Silica-based materials are often less studied than clays but hold potential as HAB mitigation agents. Pan et al. [22] demonstrated that beach sand modified with chitosan and PAC could remove 80% of *Amphidinium carterae Hulburt* and *Chlorella sp.* in just 3 minutes, where chitosan enhances floc formation and sand serves as ballast for sedimentation. In addition, the chitosan also functions as an electrostatic trap to prevent the cells from escaping from the flocs. The sand acted as ballast for sedimentation. Chen & Pan [23] showed that xanthan could trap the algae cells similar to chitosan, where the efficiency was enhanced in the presence of calcium hydroxide. The removal efficiency of *Amphidinium carterae* Hulburt culture increased to 83–89% within 30 min using 300 mg L^{-1} clays, soils, or sands modified with 20 mg L^{-1} xanthan and 100 mg L^{-1} calcium hydroxide ($Ca(OH)_2$). By comparison, only 55% of removal was achieved when xanthan was used without $Ca(OH)_2$. The addition of

$Ca(OH)_2$ decreased the repulsive interaction between anionic xanthan and negatively charged algal cells, attributed to salt-bridging effects due to Ca^{2+}. Jin et al. [24] investigated the potential of bicomponent modified soil using amphoteric starch (AS) and PAC for the mitigation of *Microcystis aeruginosa* and marine *Chlorella* sp. The removal efficiency contributed to 99.9% in fresh and saline waters, and *Chlorella* sp. in marine water. Diaz et al. [25] developed a novel silica-based antimicrobial nanofilm using a composite of silica-modified quaternary ammonium compounds, didecyldimethylammonium chloride solution (Fixed-Quat) applied to a fibreglass mesh for the mitigation of *Microcystis aeruginosa*. More than 99% of *Microcystis aeruginosa* was removed after 10 hr of exposure. The inhibition is attributed to the electrostatic attraction between the negatively charged algae and the alkyl chain of the Fixed-Quat, which can disrupt the cytoplasmatic membrane and result in killing of the algae.

Despite their effectiveness, modified clays and sands, raise concerns about their long-term ecological impact due to sedimentation and the introduction of non-native materials [26]. An alternative approach involves integrating these agents into chitosan-based films, which can trap algal cells and be recovered for disposal after the HAB season. However, traditional chitosan films tend to be brittle, necessitating the use of reinforcing agents to improve their mechanical and physical properties [27,28]. This study addresses existing research gaps by developing an innovative, eco-friendly silica/chitosan composite film reinforced with (3-glycidyloxypropyl) triethoxysilane (GPTEOS) and glycerol for the mitigation of *Alexandrium minutum* (*A. minutum*). By utilizing silica derived from rice husk, a sustainable and abundant agricultural byproduct rich in amorphous silica (~90%), the study not only contributes to harmful algal bloom (HAB) mitigation but also promotes agricultural waste valorisation. The incorporation of GPTEOS and glycerol enhances the film's flexibility and processability, overcoming the brittleness typically associated with chitosan-based materials. Additionally, the

recoverable nature of the films prevents sedimentation issues commonly observed with conventional clay- and silica-based treatments, offering a more sustainable and efficient approach to HAB control.

2 Materials and Methods

2.1 Materials

Rice husk was sourced from a rice mill in Penang, Malaysia. The following chemicals were used without further purification: hydrochloric acid (37%, Sigma-Aldrich, United States), chitosan powder (medium molecular weight, product ID: 448877, Sigma-Aldrich, United States), nitric acid (65%, Qrec, Malaysia), sodium hydroxide pellets (99%, Qrec, Malaysia), glacial acetic acid (100%, Qrec, Malaysia), glycerol (99.5%, Qrec, Malaysia), glycerol and (3-glycidyloxypropyl)triethoxysilane (GPTEOS, >98%, Sigma-Aldrich, United States). Filtered seawater for the mitigation studies was provided by the Fisheries Research Institute (FRI) in Batu Maung, Penang, Malaysia.

2.2 Preparation of rice husk ash

Rice husk ash (RHA) was prepared following the method described by Adam et al. [29]. First, the rice husk (RH) was thoroughly washed with distilled water to remove dirt and then air-dried for 48 h at room temperature. To eliminate metallic impurities, 30 g of cleaned RH was soaked in 750 mL of 1.0 M HNO_3 and agitated at room temperature for 24 h. Afterwards, the acid-treated RH was rinsed with distilled water until the filtrate was clear and then dried at 100°C for 24 h. Finally, the dried RH was calcined in a furnace at 600°C for 6 h, resulting in white RHA.

2.3 Preparation of sodium silicate solution

A sodium silicate solution was prepared following the method described by Sumarni et al. [30] with some modifications. Rice husk ash (RHA, 3 g) was dissolved in 350 mL of 1.0 M NaOH

and stirred at 70°C for 6 h. The resulting semi-dried material was calcined at 600°C for 30 min to produce sodium silicate powder. Subsequently, 1.71 g of the powder was dissolved in 200 mL of distilled water to obtain a clear sodium silicate solution.

2.4 Synthesis of chitosan/silica films

Composite films were synthesized following the method by Liu et al. [31] with some modifications. A 2% w/v chitosan solution was prepared by dissolving 2 g of chitosan powder in 100 mL of 1% v/v acetic acid solution. The mixture was stirred at 50°C for 4 h, then centrifuged at 4000 rpm for 15 min, and filtered to remove any undissolved chitosan. To the filtered chitosan solution, 3 mL of sodium silicate solution and 3 mL of either glycerol or (3-(glycidyloxypropyl)triethoxysilane) (1% v/v) were added. The solution was stirred for 2 h to achieve homogeneity and minimise bubble formation. This film-forming solution was poured into a square Teflon mould and dried in an oven at 50°C for 21 h. A 2% w/v sodium hydroxide (NaOH) solution was prepared by dissolving 10 g of NaOH pellets in 500 mL of distilled water. The dried film was soaked in this NaOH solution for 1 min and then rinsed with distilled water to neutralize it. Finally, the film was air-dried at room temperature for 24 h and stored in a desiccator for later use. The films incorporating glycerol and (3-(glycidyloxypropyl)triethoxysilane) were labelled as CHT/SiO_2/Gly and CHT/SiO_2/GPTEOS, respectively. Digital images of the films are shown in Fig. S1 in the Supplementary Material.

2.5 Characterizations

The surface topology of the films was analysed using a scanning electron microscope (SEM Leica Cambridge S360). Bruker-D8 Advance Powder X-ray diffraction (XRD) was used to determine the films' crystalline phases and degree of crystallinity at 2θ angle of 5º to 50º. The films' swelling index (SI) was conducted by submerging the pre-weighed dry films into 100 mL of seawater for 24 h at room temperature. Thereafter, the swollen films were removed,

wiped with filter paper to remove excess water and weighed. The SI was estimated with Equation (1) as reported by Liu et al.[31] and Sabzevari et al.[32] by employing three film samples to obtain the triplicate average. The algal medium pH before and after film immersion was recorded using a pH meter (Model Hanna edge^{pH}).

$$S_i\,(\%) = \frac{W_f - W_i}{W_i} \times 100\% \qquad (1)$$

where W_f is the weight of the swollen film after 24 h and W_i is the weight of the dry film before immersion.

The film's wettability or water contact angle (CA) was tested via the static CA using a goniometer (Rame'-Hart Instrument Co., United States) based on the sessile drop method. Deionised water (4 µL) was dropped using a micro syringe onto the smooth surface of the film at room temperature. Then, a microscope was used to capture the micrograph images. This step was repeated for five different spots of the films to calculate the average CA.

2.6 Mitigation studies

The mitigation studies were carried out at the Fisheries Research Institute (FRI) in Batu Maung, Penang, Malaysia, using *A.minutum* culture in the mid to late exponential growth phase as the source of HABs. The experiments were conducted in 250 mL beakers, each containing 150 mL of cell cultures at a concentration of 20,000 cells/mL.

In a typical mitigation experiment, the films were tied to a rod and hung vertically with three-quarters of the film immersed into the cell cultures for the moving cells to be adsorbed. The experimental set-up is shown in Fig. S2 in the Supplementary Material. The beakers were placed on the table under static condition. Approximately 1 mL samples from 2 cm below the liquid surface were collected and preserved with one drop of Lugol's solution at each specific time interval. The removal efficiency was determined for 72 h. The preserved cells were

counted using the Sedgwick-rafter counter under a light microscope (Leica CME) at 10x magnification. The effects and changes of the cells on the surface of the films were also observed under the Digital microscope (Keyence VHX E-100). Removal efficiency rate (RE) was calculated using Equation (2) [33]. All the RE data were expressed as the mean ± standard deviation (S.D).

$$RE(\%) = 1 - \left[\frac{Final\ cell\ concentration\ in\ sample}{Final\ cell\ concentration\ in\ control}\right] \times 100\% \quad (2)$$

2.7 Biodegradation of films in the soil

The biodegradability of the films was assessed through a soil burial test. Natural soil was placed in a plastic container at a depth of 20 cm, and the films were buried at a depth of 15 cm for a duration of 30 days. The containers were positioned in an open environment to allow exposure to natural climatic conditions. At 7-day intervals, the films were retrieved, gently cleaned with filter paper to remove adhering soil, and dried at 60°C for 6 h. The weight loss of the films (I_s) was measured at each time point to evaluate the extent of degradation. Additionally, physical changes in the films were documented. The percentage of degradation was determined using Equation (3).

$$I_s(\%) = \frac{W_f - W_i}{W_i} \times 100\% \quad (3)$$

where W_i and W_f are the initial weight and final weight of the film at different burial times, respectively.

3 Results and Discussion

3.1 Characterization of The Films

Figure 1(a) presents the XRD diffractograms of CHT/SiO_2/Gly and CHT/SiO_2/GPTEOS. Three distinct diffraction peaks are observed at 2θ = 10.1°, 20.1°, and 21.8°, corresponding to

the (002), (101), and (220) crystallographic planes of chitosan, respectively. The peak at 2θ = 10.1° is attributed to the hydrated crystallite structure of chitosan, caused by the incorporation of water molecules into the crystal lattice. Meanwhile, the peak at 2θ = 20.1° is associated with the regular crystalline lattice of chitosan, and the peak at 2θ = 21.8° represents its amorphous structure [34]. The appearance of this peak suggests that the crosslinking interactions between chitosan and glycerol or GPTEOS are sufficiently strong to alter its crystalline structure [35-37]. Additionally, the broadness of the peaks in the range of 2θ = 22° ~ 30° are indicative of the amorphous silica (SiO_2) present in the films [38,39].

The ATR-FTIR spectra of the films are presented in Fig. 1(b). The peak at 1016 cm^{-1}corresponds to the symmetric stretching of the C-O-C bond, while the peak at 1075 cm^{-1} is attributed to the skeletal vibration of C-O, commonly recognised as the fingerprint peak of the chitosan structure. The IR peak at 1554 cm^{-1} is associated with the -NH bending and -CN stretching vibrations, characteristic of the amide II region [40,31], whereas the peak at 1645 cm^{-1} corresponds to the -C=O stretching of amide I [40]. Peaks at 1384 $cm^{-1}$and a shoulder at 1317 cm^{-1} indicate asymmetric -C-O-C and -C-O stretching vibrations of the CH-OH group, respectively. The broad IR band observed between 3000 and 3500 cm^{-1} reflects the asymmetric and symmetric stretching vibrations of the -NH bond, as well as the Si-OH bond stretching and adsorbed water (H-O-H) on the silica surface [41]. The peak at 2876 cm^{-1} is attributed to the asymmetric stretching of $-CH_2$. Peaks in the 1000-1100 cm^{-1} range are associated with Si-O-Si bonds [42]. In the spectrum of CHT/SiO_2/Gly, the bending vibration of C-OH appears around 1416 cm^{-1}, while the peak at 1362 cm^{-1} corresponds to the C-H vibration of glycerol [43].

The reaction mechanisms between silica, chitosan, glycerol, and GPTEOS were proposed based on the FTIR findings. Crosslinking between chitosan and silica occurs via

condensation reactions between Si-OH groups on silica and hydroxyl (-OH) groups on chitosan, forming Si-O-C bonds. These bonds are typically observed near 1252 cm^{-1} [44] and are challenging to distinguish due to spectral overlap. Additionally, hydrogen bonding between Si-OH groups and chitosan amine groups is favourable [45], as illustrated in Fig. S3 in the Supplementary Material.

In the case of CHT/SiO_2/Gly, physical crosslinking occurs via hydrogen bonding between the -OH groups of glycerol with the -OH and amine groups of the chitosan/silica composite, as shown in Fig. S4 in the Supplementary Material [46]. For CHT/SiO_2/GPTEOS, the proposed mechanism in Fig. S5 in the Supplementary Material involves hydrolysis of GPTEOS to form an organosilicon intermediate **(A)**, which reacts with silanol groups via condensation to produce an intermediate **(B)**. Subsequently, the epoxy ring of intermediate **(B)** cleaves and reacts with the amine groups of chitosan. Additional hydrogen bonding between the -OH groups of intermediate **(B)** and chitosan further stabilises the structure.

Figure 2 displays the SEM images of CHT/SiO_2/Gly and CHT/SiO_2/GPTEOS, illustrating surface morphology and cross-sectional structures. The surfaces of CHT/SiO_2/Gly (Fig. 2(a)) and CHT/SiO_2/GPTEOS (Fig. 2(c)) appear heterogeneous. Cross-sectional images (Fig. 2(b) and (d)) reveal the presence of microcracks and voids, which are more prominent in CHT/SiO_2/Gly compared to CHT/SiO_2/GPTEOS. The greater intensity and broadness of the IR peak at 3000–3500 cm^{-1} for CHT/SiO_2/Gly indicate a higher concentration of -OH bonds. These bonds promote hydrogen bonding within the biopolymer network, which can induce an anti-plasticizing effect, rigidifying the biopolymer structure. This tighter network is likely responsible for the microcracking observed in the cross-sectional image of CHT/SiO_2/Gly. The voids and microcracking are a direct result of the stress induced by the less stable network due to hydrogen bonding [47]. In contrast, the cross-section of CHT/SiO_2/GPTEOS (Fig. 2(d))

shows fewer microcracks and voids, suggesting a denser structure with greater stability. This difference can be attributed to the reduced presence of -OH bonds in CHT/SiO_2/GPTEOS, which minimizes the anti-plasticizing effect and results in a more stable biopolymer network without significant structural disruptions.

The wettability test evaluates the extent of wetting when solid and liquid phases interact, as determined by the contact angle between a water droplet and the film surface. A contact angle $\leq 90°$ indicates greater wettability, while a contact angle $\geq 90°$ signifies reduced wettability [48]. As illustrated in Fig. 3, the contact angle of CHT/SiO_2/Gly ($58.28 \pm 0.03°$) is lower than that of CHT/SiO_2/GPTEOS ($84.92 \pm 0.05°$), suggesting higher wettability for CHT/SiO_2/Gly.

As observed in the FTIR analysis, CHT/SiO_2/Gly may contain a higher concentration of -OH groups, facilitating the formation of hydrogen bonds between water molecules and the film's surface, thereby enhancing wettability. In contrast, the higher contact angle of CHT/SiO_2/GPTEOS is due to the reduced presence of -OH groups, which limits hydrogen bonding with water molecules and decreases its wettability.

Blending chitosan with other components typically increases the film's thickness. However, in this study, the thickness of the films remained relatively unchanged, as shown in Table 1. This is attributed to the incorporation of silicate species within the chitosan framework, which results in tighter binding and a more compact film structure [49]. In CHT/SiO_2/Gly, the hydrodynamic radius of glycerol (0.28 nm-0.71 nm depending on the method of determination and the specific conditions of the measurement) resulted in an increase of the spacing between chitosan macromolecules within each layer without significantly separating them [50-52]. The plasticizer molecules form hydrogen bonds with specific sites on the polymer (-OH, -NH_2), which stabilizes the structure and prevent a

significant increase in thickness. In CHT/SiO_2/GPTEOS, higher crosslinking causes the chitosan macromolecular layers to pack more closely together.

The swelling index of the films is also presented in Table 1 which indicates that CHT/SiO_2/Gly has a higher swelling index than CHT/SiO_2/GPTEOS. This is due to the abundance of functional groups, such as -OH and -NH_2, in CHT/SiO_2/Gly, which readily form hydrogen bonds with water molecules [53]. These functional groups promote water uptake, increasing the swelling capacity [54,55]. In contrast, CHT/SiO_2/GPTEOS exhibits a lower swelling index due to the hydrophobic nature of GPTEOS. During the crosslinking reaction, many of GPTEOS's functional groups are utilised, further enhancing its hydrophobicity and reducing its ability to interact with water.

The point of zero charge (PZC) is the pH at which the surface charge of a material is neutral, meaning the positive and negative surface charges are equal under specific conditions of temperature, pressure, and solution composition [56]. It does not imply the absence of surface charges but rather a balance between opposing charges [57]. The pH_{PZC} values for CHT/SiO_2/Gly and CHT/SiO_2/GPTEOS were determined to be 4.39 and 4.27, respectively, as shown in Fig. 4.

3.2 Algae Control and Mechanism

The mitigation of *A. minutum* using the films was evaluated, and the removal efficiency (RE) is shown in Fig. 5. During the first 3 h, the RE fluctuated between 18.1 ± 9.81% and 25.9 ± 10.16%. The trend suggests that the physical properties of the films, particularly their swelling behaviour play a key role in the early interactions with the algae. The swelling of the films alters their porosity, initially allowing algae cells to be captured but also enabling some to escape. The lower swelling index of CHT/SiO_2/GPTEOS may have contributed to its higher

RE, as it maintained a more stable structure for cell adhesion. Between 10 h and 20 h, the RE values increased significantly, indicating a more effective algae entrapment and interaction, but subsequently declined and fluctuated until the end of the experiment. After 72 h, CHT/SiO_2/Gly achieved an RE of 26.5 ± 10.81%, while CHT/SiO_2/GPTEOS exhibited a higher RE of 50.06 ± 11.90%. Statistical analysis confirmed that the differences between the films were significant ($p < 0.05$).

Compared to previously reported silica-based mitigation agents (Table 2), the removal efficiency (RE) of CHT/SiO_2/Gly and CHT/SiO_2/GPTEOS was lower, which can be attributed to several factors. The continuous swelling of the films throughout the study may have caused initially absorbed algae cells to detach and escape into the seawater, reducing overall retention. Additionally, the surface charge properties of the films, influenced by their pH, played a significant role in algae adhesion. The pH_{PZC} values of CHT/SiO_2/Gly (4.39) and CHT/SiO_2/GPTEOS (4.27) were considerably lower than the algal culture pH (8.0). Since A. minutum cells are also negatively charged, electrostatic repulsion likely limited effective interactions between the algae and the films, ultimately lowering the removal efficiency.

3.3 Characterization of the Films Post Mitigation

Digital microscopy was performed on the used films to examine the state of the algae cells post-mitigation. The images revealed that algae cells attached to the CHT/SiO_2/Gly appeared ruptured (Fig. 6(a)), while those on the CHT/SiO_2/GPTEOS (Fig. 6(b)) remained intact. This suggests that chemical interactions within the films influenced the mode of algae inhibition. Algae cells possess various functional groups such as hydroxyl (-OH) and carboxyl (-COOH), which can react with the films' framework through hydrogen bonding [58]. As previously discussed, the amine groups in CHT/SiO_2/GPTEOS were involved in crosslinking, reducing

their accessibility, whereas those in CHT/SiO_2/Gly remained free. This allowed greater electrostatic stress upon attachment, leading to cell rupture[21, 52].

As shown in Fig. 7(a), the surface of CHT/SiO_2/Gly exhibited aggregated cell debris, likely originating from ruptured algae cells. In contrast, the surface of CHT/SiO_2/GPTEOS displayed irregularly shaped particles. These differences in morphology further support that stronger physical interactions and possible oxidative stress mechanisms contributed to algae removal. However, it is important to note that the observed structural changes in algae cells might have been influenced by the drying process used before SEM imaging.

3.4 Biodegradation of the Used Films in The Soil

Chitosan is widely recognized for its biocompatibility and biodegradability, which were key factors in evaluating the algae-laden films' degradation in soil over a month-long interval. Physical changes in the buried films were documented through photographs, with notable degradation highlighted by red circles in Fig. 8. After 7 days of burial, the films became brittle and began fragmenting, and by day 30, they had completely degraded. This rapid degradation highlights the films' environmentally friendly nature, enabling safe disposal without contributing to aquatic pollution. The ability of the films to absorb water and swell enhances the solubility of the chitosan and accelerates biodegradation by promoting faster microbial colonization and degradation. Soil-inhabiting organisms such as *Serratia marcescens*, *Pseudomonas aeruginosa*, and *Beauveria bassiana*, can effectively degrade chitosan-containing films as a carbon and nitrogen source [60,61].

4 Conclusion

This study presents a promising approach for the mitigation of *A. minutum* using an eco-friendly silica/chitosan composite film reinforced with GPTEOS and glycerol. By utilizing

silica from rice husk, this method not only addresses HAB control but also contributes to agricultural waste management. The incorporation of GPTEOS and glycerol enhances the flexibility and processability of the films, mitigating the brittleness commonly associated with chitosan-based materials. Furthermore, the recoverable nature of the films prevents sedimentation issues associated with traditional clay- and silica-based mitigation agents.

The films demonstrated different removal efficiency, with CHT/SiO_2/Gly achieving 26.57 ± 10.81% and CHT/SiO_2/GPTEOS reaching 50.06 ± 11.90%. The differences in performance were attributed to the structural and chemical properties of the films, including the swelling properties. CHT/SiO_2/GPTEOS exhibited superior mitigation efficiency due to its lower ability to swell. Both films were highly biodegradable, completely decomposing within 30 days of burial in the soil profile. While the removal efficiency observed in this study is lower than that of some previously reported methods, further optimization of the film composition and surface charge properties could enhance performance. Future studies will focus on optimizing the glycerol-to-GPTEOS ratio to improve swelling behaviour, reducing algae cell escape and increasing capture efficiency. Additionally, incorporating advanced characterization techniques and biodegradation studies under simulated aquatic conditions will provide deeper insights into the film's long-term environmental impact. With further refinements, this approach holds significant potential as a sustainable and effective strategy for HAB mitigation.

Acknowledgements

The authors would like to thank Universiti Sains Malaysia for funding this research through Geran Penyelidikan Jangka Pendek-Jordan (R501-LR-RND002-0000000130-0000) and also Fisheries Research Institute (FRI), Department of Fisheries Malaysia, Batu Maung, Penang for granting the permission to use their facilities to conduct mitigation studies. Anwar Iqbal would like to thank the National Research and Innovation Agency (BRIN), Government of the

Republic of Indonesia for the appointment as a visiting researcher during the sabbatical program.

Supplementry data

The Supplementry data is available at:

file:///C:/Users/pc/Downloads/Supplementary-%20Iqbal%20(70-SCI-2501-9854).pdf

References

1. Anderson, D. M. "Approaches to monitoring, control and management of harmful algal blooms (HABs)", *Ocean Coast. Manag.* **52** (7), 342–347 (2009). https://doi.org/10.1016/j.ocecoaman.2009.04.006.

2. Hoagland, P., Anderson, D. M., Kaoru, Y. and White, A. W. "The economic effects of harmful algal blooms in the united states: estimates, assessment issues, and information needs", *Estuaries*, **25** (4), 819–837 (2022). https://doi.org/10.1007/BF02804908.

3. Armstrong, A., Stedman, R. C., Sweet, S., et al. "What causes harmful algal blooms? A case study of causal attributions and conflict in a lakeshore community", *Environ. Manage.*, **69** (3), 588–599 (2022). https://doi.org/10.1007/s00267-021-01581-9.

4. Balaji-Prasath, B., Wang, Y., Su, Y. P., et al. "Methods to control harmful algal blooms: a review", *Environ. Chem. Lett.* **20**, 3133–3152 (2022). https://doi.org/10.1007/s10311-022-01457-2.

5. Anderson, D. M., Fensin, E., Gobler, C. J., et al. "Marine Harmful Algal Blooms (HABs) in the United States: History, Current Status and Future Trends", *Harmful Algae*, **102**, 101975 (2021). https://doi.org/10.1016/j.hal.2021.101975.

6. Bresnan, E., Arévalo, F., Belin, C., et al. "Diversity and regional distribution of harmful algal events along the Atlantic margin of Europe", *Harmful Algae*, *102*, 101976 (2021). https://doi.org/10.1016/j.hal.2021.101976.

7. Carias, J., Vásquez-Lavín, F., Barrientos, M., et al. "Economic Valuation of Harmful Algal Blooms (HAB): Methodological challenges, policy implications, and an empirical application", *J. Environ. Manage.* **365**, 121566 (2024). https://doi.org/10.1016/j.jenvman.2024.121566.

8. Melaram, R., Newton, A. R., Lee, A., et al. "A review of microcystin and nodularin toxins derived from freshwater cyanobacterial harmful algal blooms and their impact on human health", *Toxicol. Environ. Health Sci.* , **16** (3), 233–241 (2024). https://doi.org/10.1007/s13530-024-00220-0.

9. Anderson, D. M. "Harmful algal blooms. In *Encyclopedia of Ocean Sciences*", Elsevier, pp 309–321 (2019). https://doi.org/10.1016/B978-0-12-409548-9.11468-X.

10. Li, X.-Y., Yu, R.-C., Richardson, A. J., et al. "Marked shifts of harmful algal blooms in the bohai sea linked with combined impacts of environmental changes", *Harmful Algae*, *121*, 102370 (2023). https://doi.org/10.1016/j.hal.2022.102370.

11. Xiao, Z., Tan, A. X., Xu, V., Jun, Y.-S. et al. "Mineral-hydrogel composites for mitigating harmful algal bloom and supplying phosphorous for photo-biorefineries", *Sci. Total Environ. 847*, 157533 (2022). https://doi.org/10.1016/j.scitotenv.2022.157533.

12. Glibert, P. M. "Harmful algae at the complex nexus of eutrophication and climate change", *Harmful Algae*, **91**, 101583 (2020). https://doi.org/10.1016/j.hal.2019.03.001.

13. Zahir, M., Su, Y., Shahzad, M. I., et al. "A review on monitoring, forecasting, and early warning of harmful algal bloom", *Aquaculture*, *593*, 741351 (2024). https://doi.org/10.1016/j.aquaculture.2024.741351.

14. Hallegraeff, G. M., Anderson, D. M., Belin, et al. "Perceived global increase in algal blooms is attributable to intensified monitoring and emerging bloom impacts", *Commun. Earth Environ.* **2** (1), 117 (2021). https://doi.org/10.1038/s43247-021-00178-8.

15. Yu, Z., Zou, J. and Ma, X., et al., "Controlling red tide by means of chemistry", *Oceanol. et Limnol. Sinica*, **24**(3): 314–318 (1993). (in Chinese with English abstract).

16. Li, H., Yu, Z., Cao, X. et al. "Chitosan modification and its synergism with clay to mitigate harmful algal blooms", *Environ. Technol. Innov.*, **29**, 103028 (2023). https://doi.org/10.1016/j.eti.2023.103028.

17. Rosa, M., Ward, J. E., Holohan, et al. "Physicochemical surface properties of microalgae and their combined effects on particle selection by suspension-feeding bivalve molluscs", *J. Exp. Mar. Biol. Ecol.*, **486**, 59–68 (2017). https://doi.org/10.1016/j.jembe.2016.09.007.

18. Yu, Z. and Sun, X. "Effects of e-e interaction on the cdw of mx complex", *Chin. Phys. Lett.* **11** (2), 105–108 (1994). https://doi.org/10.1088/0256-307X/11/2/012.

19. Yu, Z., Song, X., Cao, X. et al. "Mitigation of harmful algal blooms using modified clays: theory, mechanisms, and applications", *Harmful Algae*, 69, 48–64 (2017). https://doi.org/10.1016/j.hal.2017.09.004.

20. Chi, L., Shen, H., Jiang, K., et al. "BTXs removals by modified clay during mitigation of *Karenia Brevis* Bloom: insights from adsorption and transformation", *Chemosphere*, **362**, 142668 (2024). https://doi.org/10.1016/j.chemosphere.2024.142668.

21. Zhang, H., Zhang, Y., Wang, C., et al. “Study on the kinetic mechanism of hydrodynamically enhanced modified clay removal of aphanizomenon flos-aquae: from laboratory to field engineering applications”, *Sep. Purif. Technol. 340,* 126651 (2024). https://doi.org/10.1016/j.seppur.2024.126651.

22. Pan, G., Chen, J. and Anderson, D. M. “Modified local sands for the mitigation of harmful algal blooms”, *Harmful Algae***,** *10* (4), 381–387 (2011). https://doi.org/10.1016/j.hal.2011.01.003.

23. Chen, J. and Pan, G. “Harmful algal blooms mitigation using clay/soil/sand modified with xanthan and calcium hydroxide”, *J. Appl. Phycol.24* (5), 1183–1189 (2012). https://doi.org/10.1007/s10811-011-9751-7.

24. Jin, X., Bi, L., Lyu, T., et al. “Amphoteric starch-based bicomponent modified soil for mitigation of harmful algal blooms (HABs) with broad salinity tolerance: flocculation, algal regrowth, and ecological safety”, *Water Res.*, **165**, 115005 (2019). https://doi.org/10.1016/j.watres.2019.115005.

25. Diaz, D., Church, J., Young, M. et al. “Silica-quaternary ammonium “fixed-quat” nanofilm coated fiberglass mesh for water disinfection and harmful algal blooms control”, *J. Environ. Sci.*, **82**, 213–224 (2019). https://doi.org/10.1016/j.jes.2019.03.011.

26. Cao, S., Liu, Z., Zhou, B., et al. “Post-ecological effect and risk assessment of using modified clay in harmful algal bloom mitigation: an attempt based on the responses of zooplankton *Brachionus Plicatilis* and Bivalve *Mytilus Edulis*”, *Ecotoxicol. Environ. Saf.,* **230**, 113134 (2022). https://doi.org/10.1016/j.ecoenv.2021.113134.

27. Yu, J., Xu, S., Goksen, G., et al. “Chitosan films plasticized with choline-based deep eutectic solvents: uv shielding, antioxidant, and antibacterial properties”, *Food Hydrocoll.* **135**, 108196 (2023). https://doi.org/10.1016/j.foodhyd.2022.108196.

28. Syaubari, A., Asnawi, T. M., Zaki, et al. “Synthesis and characterization of biodegradable plastic from watermelon rind starch and chitosan by using glycerol as plasticizer”, *Mater. Today Proc.* **63**, S501–S506 (2022). https://doi.org/10.1016/j.matpr.2022.04.535.

29. Adam, F., Osman, H. and Hello, K. M. “The immobilization of 3-(chloropropyl)triethoxysilane onto silica by a simple one-pot synthesis”, *J. Colloid Interface Sci.*, **331** (1), 143–147 (2009). https://doi.org/10.1016/j.jcis.2008.11.048.

30. Sumarni, W., Iswari, R. S., Marwoto, P. et al. “Physical characteristics of chitosan-silica composite of rice husk ash”, *IOP Conf. Ser. Mater. Sci. Eng.*, **107**, 012039 (2016). https://doi.org/10.1088/1757-899X/107/1/012039.

31. Liu, Y., Cai, Z., Sheng, L., et al. “Influence of nanosilica on inner structure and performance of chitosan based films”, *Carbohydr. Polym.*, **212**, 421–429 (2019). https://doi.org/10.1016/j.carbpol.2019.02.079.

32. Sabzevari, M., Cree, D. E. and Wilson, L. D. “Mechanical properties of graphene oxide-based composite layered-materials”, *Mater. Chem. Phys.*, **234**, 81–89 (2019). https://doi.org/10.1016/j.matchemphys.2019.05.091.

33. Kim, Z.-H., Thanh, N. N., Yang, J.-H., et al. “Improving Microalgae removal efficiency using chemically-processed clays”, *Biotechnol. Bioprocess Eng.*, **21** (6), 787–793 (2016). https://doi.org/10.1007/s12257-016-0655-x.

34. Khan, A., Khan, R. A., Salmieri, S., et al.“Mechanical and barrier properties of nanocrystalline cellulose reinforced chitosan based nanocomposite films”, *Carbohydr. Polym.*, **90** (4), 1601–1608 (2012). https://doi.org/10.1016/j.carbpol.2012.07.037.

36. Madian, N. G. and Mohamed, N. “Enhancement of the dynamic mechanical properties of chitosan thin films by crosslinking with greenly synthesized silver nanoparticles”, *J. Mater. Res. Technol.,* **9** (6), 12970–12975 (2020). https://doi.org/10.1016/j.jmrt.2020.09.028.

37. Shehap, A. M., Nasr, R. A., Mahfouz, M. A. et al. “Preparation and characterizations of high doping chitosan/mmt nanocomposites films for removing iron from ground water”, *J. Environ. Chem. Eng.,* **9** (1), 104700 (2021). https://doi.org/10.1016/j.jece.2020.104700.

38. Issa, H. K., Maleki, A., Taherizadeh, A. et al. “On the structure-properties relationship of amorphous and crystalline silica nanoparticles reinforced magnesium matrix nanocomposites”, *J. Alloys Compd.***,** *924*, 166605 (2022). https://doi.org/10.1016/j.jallcom.2022.166605.

39. Kim, J., Kim, S. Y., Yang, C.-M., et al. “Possibility of recycling sio_x particles collected at silicon ingot production process as an anode material for lithium ion batteries", *Sci. Rep.*, **9** (1), 13313 (2019). https://doi.org/10.1038/s41598-019-50011-8.

40. Fernandes Queiroz, M., Melo, K., Sabry, D., et al. “Does the use of chitosan contribute to oxalate kidney stone formation?”, *Mar. Drugs*, 13 (1), 141–158 (2014). https://doi.org/10.3390/md13010141.

41. Mujeeb Rahman, P., Abdul Mujeeb, V. M., Muraleedharan, K. et al. “Chitosan/nano zno composite films: enhanced mechanical, antimicrobial and dielectric properties”, *Arab. J. Chem.*, **11** (1), 120–127 (2018). https://doi.org/10.1016/j.arabjc.2016.09.008.

42. Ellerbrock, R., Stein, M. and Schaller, J. “Comparing amorphous silica, short-range-ordered silicates and silicic acid species by FTIR”, *Sci. Rep.* **12** (1), 11708 (2022). https://doi.org/10.1038/s41598-022-15882-4.

43. Gómez-Siurana, A., Marcilla, A., Beltrán, M., Berenguer, D., et al. “TGA/FTIR study of tobacco and glycerol–tobacco mixtures”, *Thermochim. Acta*, *573*, 146–157 (2013). https://doi.org/10.1016/j.tca.2013.09.007.

44. Jung, S. S. and Oh, T. “Generation of Si-O-C Bond without Si-CH_3 bond in hybrid type SiOC film”, In *2006 IEEE Nanotechnology Materials and Devices Conference*; IEEE: Gyeongju, South Korea, pp. 462–463 (2006). https://doi.org/10.1109/NMDC.2006.4388817.

45. Das, P., Roy, M. D. and Ghosh, S. “Study on the hydrophobicity and antibacterial activity of silica sol-chitosan-HDTMS treated cotton fabric dipped in an aquas media”, *Tekstilec*, **66**, 1–14 (2023). https://doi.org/10.14502/tekstilec.65.2022094.

46. Nathan, K. G., Genasan, K. and Kamarul, T. “Polyvinyl alcohol-chitosan scaffold for tissue engineering and regenerative medicine application: a review”, *Mar. Drugs*, **21** (5), 304 (2023). https://doi.org/10.3390/md21050304.

47. Liu, H., Adhikari, R., Guo, Q., et al. “Preparation and characterization of glycerol plasticized (high-amylose) starch–chitosan films”, *J. Food Eng.* **116** (2), 588–597 (2013). https://doi.org/10.1016/j.jfoodeng.2012.12.037.

48. Sarkar, M., Hasanuzzaman, M., Gulshan, F., et al. “Surface, mechanical and shape memory properties of biodegradable polymers and their applications”. In encyclopedia of materials: plastics and polymers; Elsevier, pp 1092–1099 (2022). https://doi.org/10.1016/B978-0-12-820352-1.00050-X.

49. Yeh, J.-T., Chen, C.-L. and Huang, K.-S. “Synthesis and properties of chitosan/SiO_2 hybrid materials”, *Mater. Lett.*, **61** (6), 1292–1295 (2007). https://doi.org/10.1016/j.matlet.2006.07.016.

50. Quijadagarrido, I., Iglesiasgonzalez, V., Mazonarechederra, J.,et al. "The role played by the interactions of small molecules with chitosan and their transition temperatures. glass-forming liquids: 1,2,3-propantriol (glycerol)", *Carbohydr. Polym.*, **68** (1), 173–186 (2007). https://doi.org/10.1016/j.carbpol.2006.07.025.

51. Elamin, K. and Swenson, J. "Brownian motion of single glycerol molecules in an aqueous solution as studied by dynamic light scattering", *Phys. Rev. E.*, **91** (3), 032306 (2015). https://doi.org/10.1103/PhysRevE.91.032306.

52. Charkhesht, A., Lou, D., Sindle, B., et al. "Insights into Hydration dynamics and cooperative interactions in glycerol–water mixtures by terahertz dielectric spectroscopy", *J. Phys. Chem. B.*, **123** (41), 8791–8799 (2019). https://doi.org/10.1021/acs.jpcb.9b07021.

53. Clasen, C., Wilhelms, T. and Kulicke, W.-M. "Formation and characterization of chitosan membranes", *Biomacromolecules*, **7** (11), 3210–3222 (2006). https://doi.org/10.1021/bm060486x.

54. Palla-Rubio, B., Araújo-Gomes, N., Fernández-Gutiérrez, et al. "Synthesis and characterization of silica-chitosan hybrid materials as antibacterial coatings for titanium implants", *Carbohydr. Polym.*, **203**, 331–341 (2019). https://doi.org/10.1016/j.carbpol.2018.09.064.

55. Huang, L., Dai, T., Xuan, Y., et al. "Synergistic combination of chitosan acetate with nanoparticle silver as a topical antimicrobial: efficacy against bacterial burn infections", *Antimicrob. Agents Chemother.* **55** (7), 3432–3438 (2011). https://doi.org/10.1128/AAC.01803-10.

56. Cleaves, H. J. "Isoelectric point. In *Encyclopedia of Astrobiology*", Gargaud, M., Irvine, W. M., Amils, R., Claeys, P., Cleaves, H. J., Gerin, M., Rouan, D., Spohn, T., Tirard,

S., Viso, M., Eds.; Springer Berlin Heidelberg: Berlin, Heidelberg, pp 1541–1541 (2023). https://doi.org/10.1007/978-3-662-65093-6_819.

57. Bakatula, E. N., Richard, D., Neculita, C. M., et al. "Determination of point of zero charge of natural organic materials", *Environ. Sci. Pollut. Res.,* **25** (8), 7823–7833 (2018). https://doi.org/10.1007/s11356-017-1115-7.

58. Agatonovic-Kustrin, S., Ramenskaya, G., Kustrin, E.,et al. "New integrated HPTLC - ATR/FTIR approach in marine algae bioprofiling", *J. Pharm. Biomed. Anal.,* **189**, 113488 (2020). https://doi.org/10.1016/j.jpba.2020.113488.

59. Bhalkaran, S. and Wilson, L. "Investigation of Self-assembly processes for chitosan-based coagulant-flocculant systems: a mini-review", *Int. J. Mol. Sci.*, **17** (10), 1662 (2016). https://doi.org/10.3390/ijms17101662.

60. Kaur, R. and Chauhan, I. "Biodegradable plastics: mechanisms of degradation and generated bio microplastic impact on soil health". *Biodegradation,* **35** (6), 863–892 (2024). https://doi.org/10.1007/s10532-024-10092-3.

61. De Souza, A. M. N., Avila, L. B., Contessa, C. R., et al. "Biodegradation study of food packaging materials: assessment of the impact of the use of different biopolymers and soil characteristics", *Polymers,* **16** (20), 2940 (2024). https://doi.org/10.3390/polym16202940.

Biographies

Anwar Iqbal is an Associate Professor at the School of Chemical Sciences, Universiti Sains Malaysia (USM), Penang, Malaysia. His research focuses on material chemistry, particularly the development of sustainable materials for environmental applications, including water treatment and harmful algal bloom (HAB) mitigation.

Nur Hanisah Ibrahim is affiliated with the School of Chemical Sciences, Universiti Sains Malaysia (USM), Penang, Malaysia. Her research interests include surface chemistry and the development of eco-friendly materials for environmental remediation.

Normawaty Mohammad Noor is an expert in marine science at the Department of Marine Science, Kulliyyah of Science, International Islamic University Malaysia (IIUM), Kuantan,

Pahang, Malaysia. Her research focuses on marine ecology, algal bloom dynamics, and sustainable mitigation strategies for marine pollution.

Roziawati Mohd Razali is a researcher at the Fisheries Research Institute (FRI), Department of Fisheries Malaysia, Batu Maung, Penang, Malaysia. She specializes in aquatic ecology, fisheries management, and the impact of harmful algal blooms on marine biodiversity and aquaculture.

Dede Heri Yuli Yanto is a researcher at the Research Center for Applied Microbiology, National Research and Innovation Agency (BRIN), Indonesia, and the Research Collaboration Center for Marine Biomaterials, Indonesia. His research expertise lies in marine microbiology, bioremediation, and the development of bio-based materials for environmental applications.

Lee D. Wilson is a Professor in the Department of Chemistry at the University of Saskatchewan, Saskatoon, Saskatchewan, Canada. His research interests include adsorption science, sustainable nanomaterials, and their applications in water purification, environmental remediation, and bioresource utilization.

He Ranri is an MSc student at the School of Chemical Sciences, Universiti Sains Malaysia (USM), Penang, Malaysia. His research focuses on material synthesis, nanocomposites, and the application of biopolymers in environmental sustainability, particularly in mitigating aquatic pollution.

Figures and Tables Caption

Fig. 1. The (a) XRD diffractogram and (b) FTIR spectra of CHT/SiO_2/Gly and CHT/SiO_2/GPTEOS.

Fig. 2. SEM images of surface and cross section of CHT/SiO_2/Gly (a); magnification 9000 and (b) magnification 50000); and CHT/SiO_2/GPTEOS (c) magnification 9000 and (d) magnification 50000).

Fig. 3. Contact angle images of (a) CHT/SiO_2/Gly and (b) CHT/SiO_2/GPTEOS.

Fig. 4. The pH_{PZC} of CHT/SiO_2/Gly and CHT/SiO_2/GPTEOS .

Fig. 5. The RE value of control, CHT/SiO_2/Gly and CHT/SiO_2/GPTEOS for 72 h. The pH of the medium is 8.

Fig. 6. The digital microscopic images of the (a) CHT/SiO_2/Gly and (b) CHT/SiO_2/GPTEOS post mitigation. The algae cells are indicated using arrows.

Fig. 7. The SEM images of (a) CHT/SiO_2/Gly and (b) CHT/SiO_2/GPTEOS post-mitigation. (Magnification: 9000).

Fig. 8. Physical changes of the used (a) CHT/SiO_2/Gly and (b) CHT/SiO_2/GPTEOS within 30 days of burial. The films are indicated by the red circles.

Table 1. The obtained film thickness, density and swelling index of the film.

Table 2. Removal efficiency of different types of algae using silica-based mitigating agents.

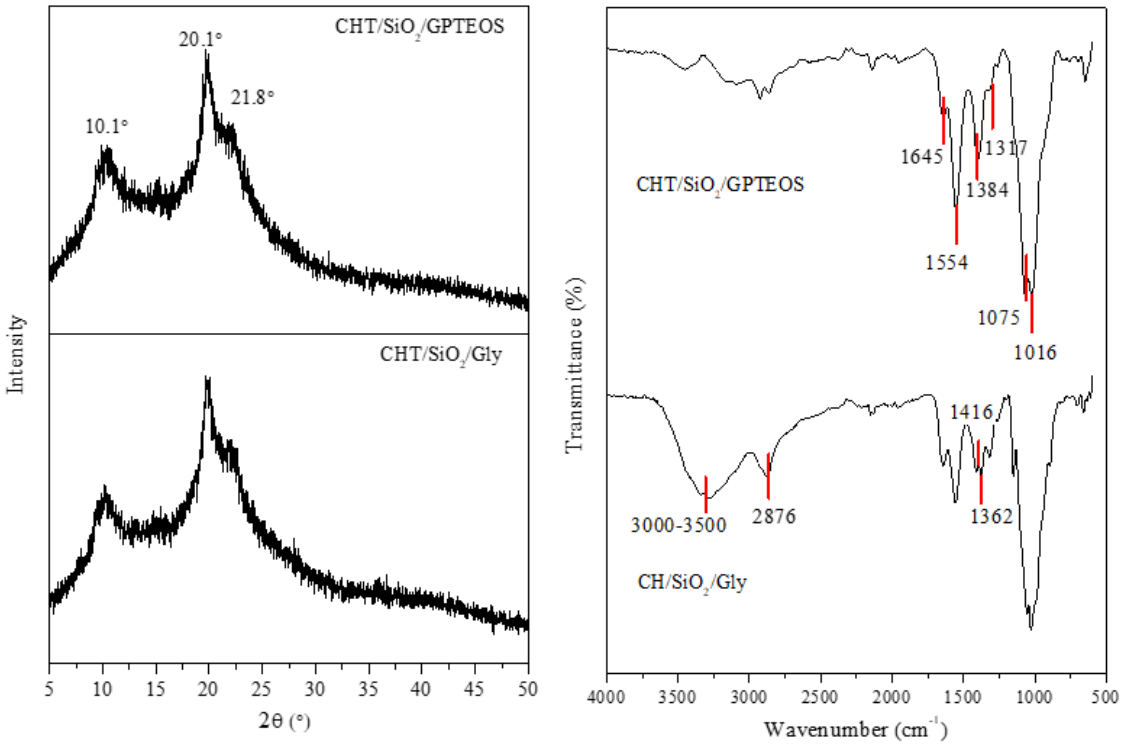

Fig. 1.

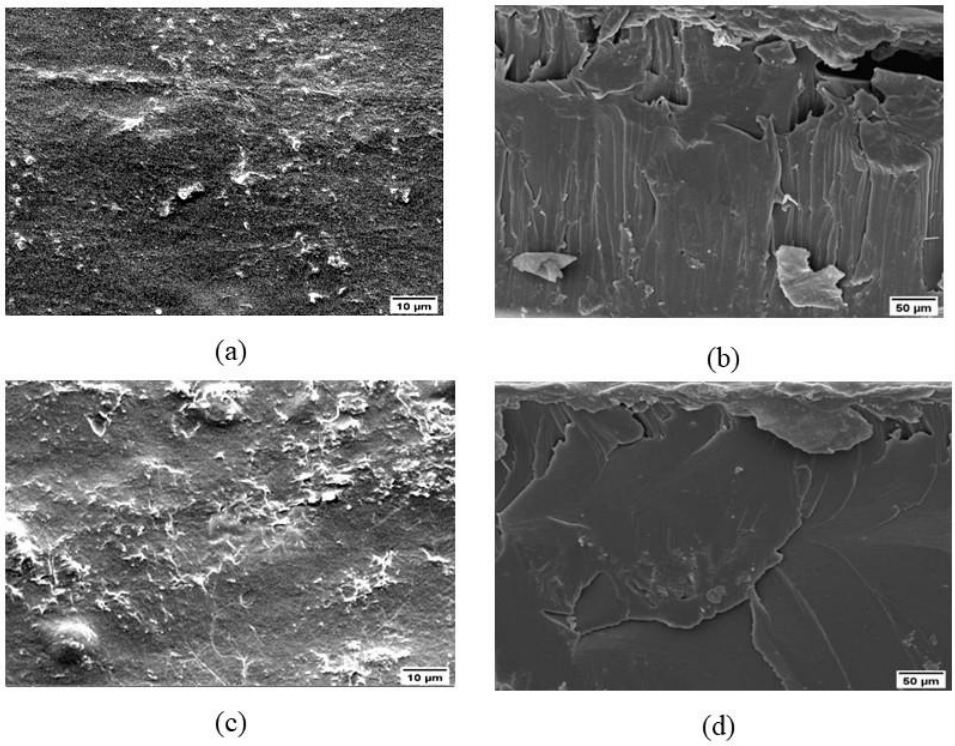

Fig. 2.

Fig. 3.

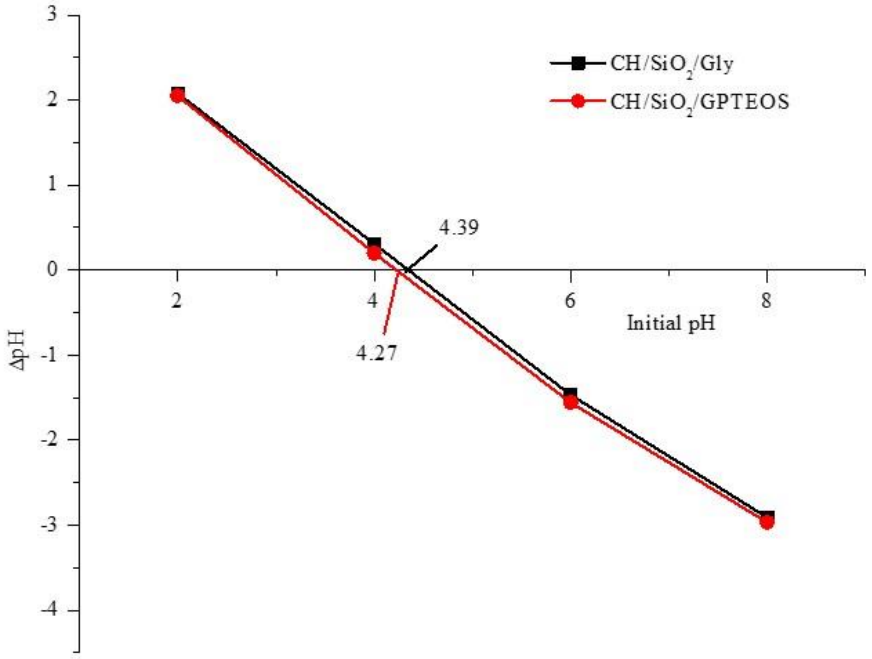

Fig. 4.

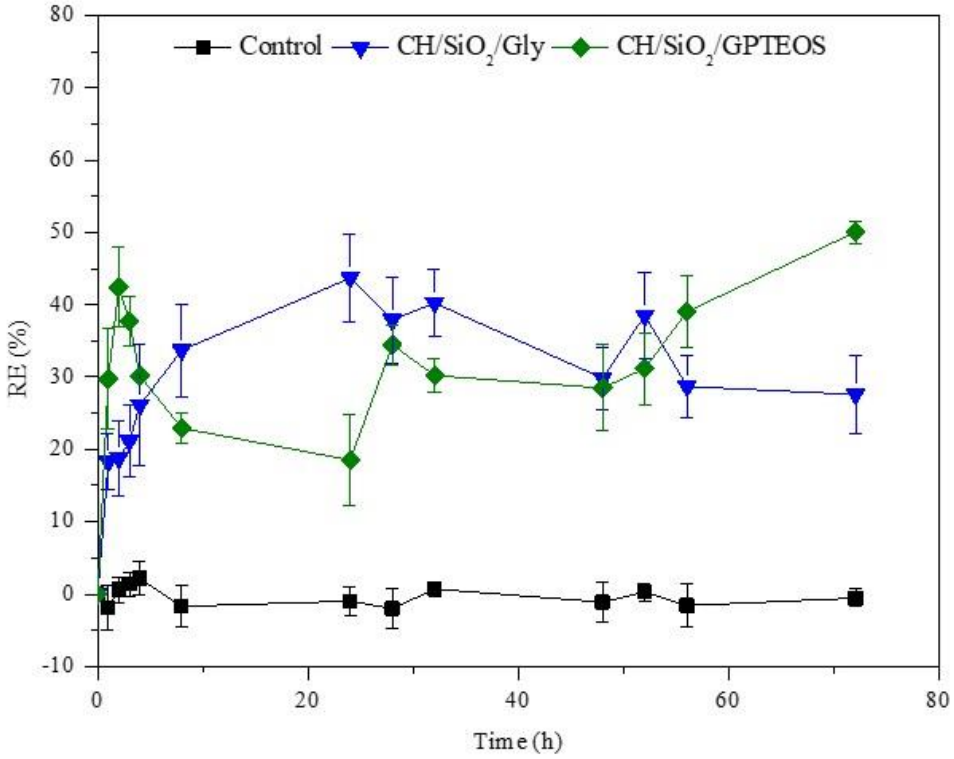

Fig. 5.

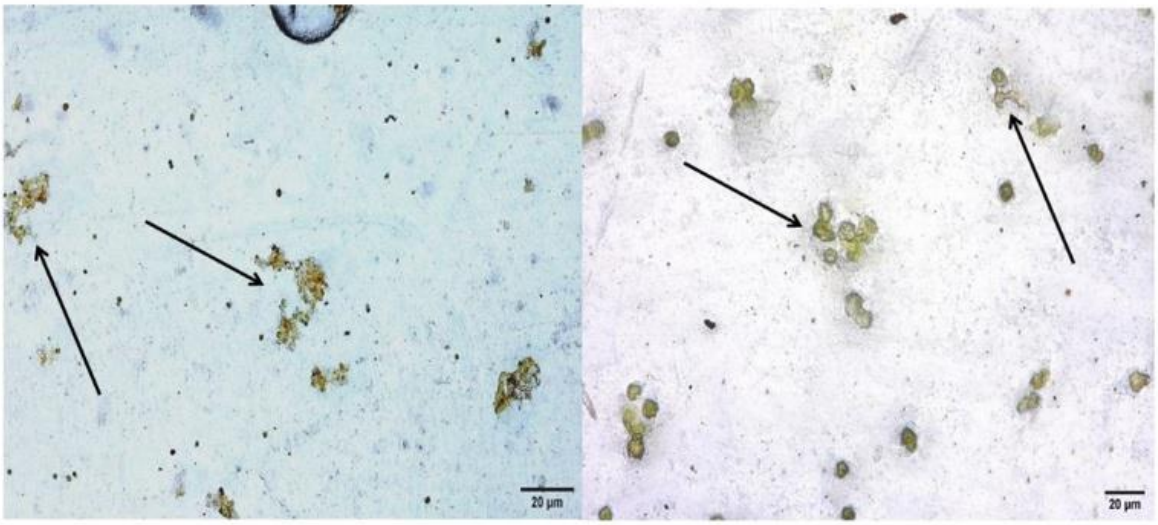

(a) (b)

Fig. 6.

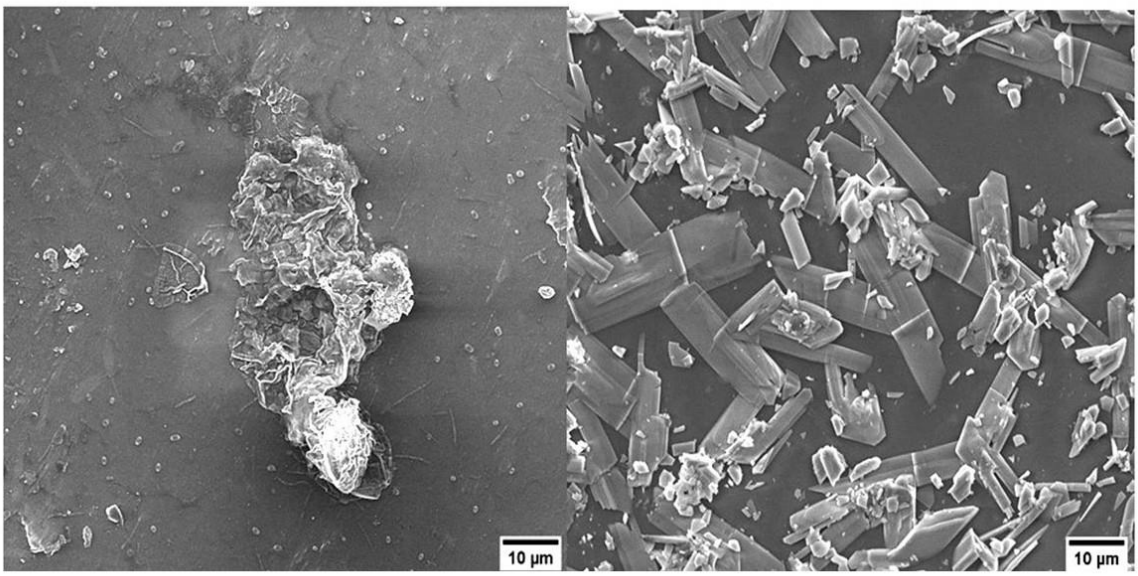

(a) (b)

Fig. 7.

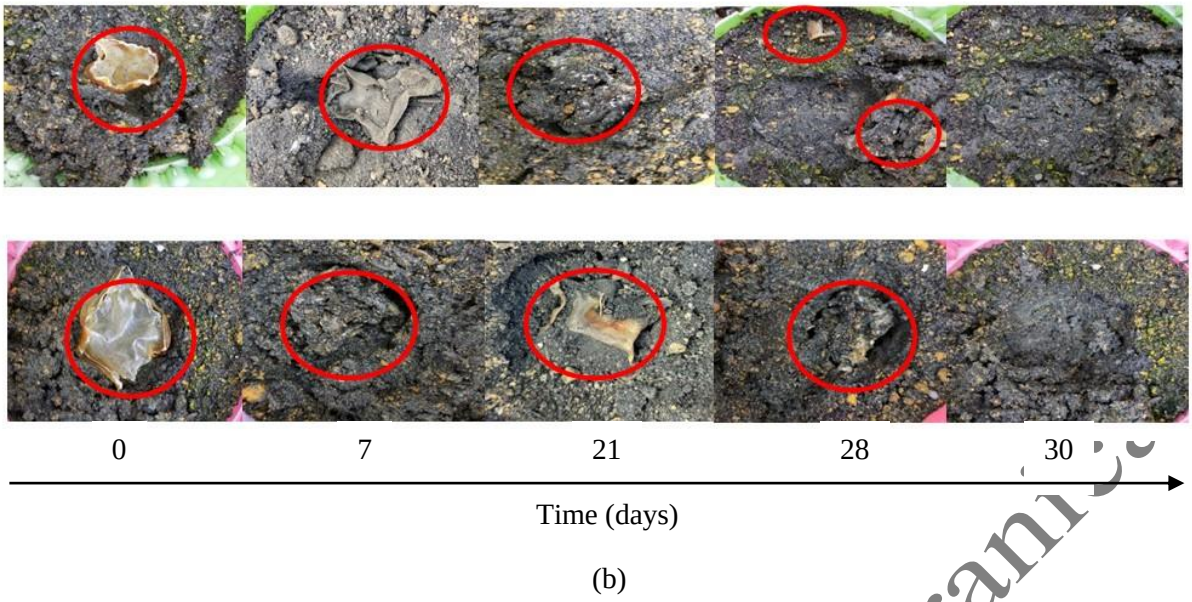

(b)

Fig. 8.

Table 1

Film type	Thickness (mm)	Swelling index (%)
CHT/SiO_2/Gly	0.366 ± 0.04	60.03 ± 1.09
CHT/SiO_2/GPTEOS	0.367 ± 0.02	45.53 ± 1.17

*The values were expressed in mean± standard deviation with significant difference ($p < 0.05$).

Table 2.

Mitigating agent	HAB species	RE	Medium pH	Time of exposure	Reference
Silica-modified QAC (Fixed-Quat) & applied to a fiberglass mesh	*Microcystis aeruginosa*	99%	-	10 h	[25]
Local beach sand or silica sand modified with chitosan & PAC.	Amphidinium *cartera e* Hulburt &Chlorella sp.	80%	8.2	3 min	[22]
Xanthane & calcium hydroxide modified clays, soils, and sands)	*Amphidinium carterae*	83–89%	-	30 min	[23]
Modified soil using amphoteric starch (AS) & PAC	*Microcystis aerugino sa*& marine Chlorella *sp.*	99.9%	3-11	5-250 min	[24]